Heat Mass Transfer (2005) 42: 112–121
DOI 10.1007/s00231-004-0611-8

ORIGINAL

Ali Al-Mudhaf · Ali J. Chamkha

Similarity solutions for MHD thermosolutal Marangoni convection over a flat surface in the presence of heat generation or absorption effects

Received: 12 May 2004 / Accepted: 19 November 2004 / Published online: 11 October 2005

Abstract The problem of steady, laminar, thermosolutal Marangoni convection flow of an electrically-conducting fluid along a vertical permeable surface in the presence of a magnetic field, heat generation or absorption and a first-order chemical reaction effects is studied numerically. The general governing partial differential equations are converted into a set of self-similar equations using unique similarity transformations. Numerical solution of the similarity equations is performed using an implicit, iterative, tri-diagonal finite-difference method. Comparisons with previously published work is performed and the results are found to be in excellent agreement. Approximate analytical results for the temperature and concentration profiles as well as the local Nusselt and sherwood numbers are obtained for the conditions of small and large Prandtl and Schmidt numbers are obtained and favorably compared with the numerical solutions. The effects of Hartmann number, heat generation or absorption coefficient, the suction or injection parameter, the thermo-solutal surface tension ratio and the chemical reaction coefficient on the velocity, temperature and concentration profiles as well as quantitites related to the wall velocity, boundary-layer mass flow rate and the Nusselt and Sherwood numbers are presented in graphical and tabular form and discussed. It is found that a first-order chemical reaction increases all of the wall velocity, Nusselt and Sherwood numbers while it decreases the mass flow rate in the boundary layer. Also, as the thermo-solutal surface tension ratio is increased, all of the wall velocity, boundary-layer mass flow rate and the Nusselt and Sherwood numbers are predicted to increase. However, the exact opposite behavior is predicted as the magnetic field strength is increased.

Keywords Marangoni convection · Magnetic field · Heat generation or absorption · Chemical reaction · Similarity solutions · Permeable surface

Nomenclature

A	temperature gradient coefficient
A^*	concentration gradient coefficient
B_0	magnetic induction
c	dimensional concentration
C	dimensionless concentration
c''	mass flux
c_p	specific heat at constant pressure
C_1	similarity transformation coefficient
C_2	similarity transformation coefficient
D	mass Diffusivity
f_0	dimensionless suction or injection velocity
$f(\eta)$	stream function similarity variable
K	dimensionless chemical reaction coefficient
m	Mass flow rate per unit width
M	Hartmann number
Ma	marangoni number, Eq. 16
Nu	Nusselt number, Eq. 34
Pr	Prandtl number
Q_0	dimensional heat generation or absorption coefficient
q''	heat flux
r	thermo-solutal surface tension ratio
R	dimensionl chemical reaction parameter
Re	Reynolds number, Eq. 18
Sc	Schmidt number
Sh	Sherwood number, Eq. 35
T	temperature
u, v	$x$component and y-component of velocity, respectively
v_0	dimensional suction or injection velocity
x, y	coordinates

Greek symbols

α	thermal diffusivity
δ	boundary layer thickness

A. Al-Mudhaf · A. J. Chamkha (✉)
Manufacturing Engineering Department,
The Public Authority for Applied Education and Training,
42325, Shuweikh, 70654, Kuwait

Δ	fluid electrical conductivity
η	location similarity variable
ϕ	dimensionless heat generation or absorption coefficient
λ	thermal conductivity
μ	dynamic viscosity
ν	kinematic viscosity
θ	temperature similarity variable
ρ	density
σ	surface tension
ψ	stream function

Subscripts

L	average over surface length
T	thermal quantity
C	solutal quantity
x	local value

1 Introduction

The existence of dissipative layers, which may occur along the liquid–liquid or liquid–gas interfaces seems to have been first observed by Napolitano [1, 2] and were called Marangoni boundary layers. Problems of this type are of great importance due to their relevance in several fields of microgravity sciences and space processing. The surface tension gradients that are responsible for Marangoni convection can be due to gradients of temperature and/or concentration (thermal/or solutal concentration). The significance of dissipative layers in liquid metal and semiconductor processing is shown to be particularly strong and is a major factor in guiding the control of industrial processes. However, although much progress have been made, especially in the study of the Marangoni convection, the state of the art is still somewhat unsatisfactory in what concerns preliminary questions of general and basic nature.

It was shown by Napolitano [3] that, much as for classical boundary layers (non-Marangoni layers), the field equations in the bulk fluids do not depend explicitly on the geometry of the interface when using as coordinates the arc length (x) and the distance normal to the interface involves however the mean curvature of its hydrostatic and dynamic shapes and, together with the other surface balance equations, introduces kinematic, thermal and pressure couplings for the flow fields in the two fluids. Napolitano and Golia [4] have shown that the fields are uncoupled when the momentum and energy resistivity ratios of the two layers and the viscosity ratio of the two fluids are much less than one. Similar solutions of Marangoni boundary layers exist when the interface temperature gradient varies as a power of the interface arc length (x). The power laws for all other variables, including the mean curvature, where determined. Numerical solutions were found, analyzed and discussed on Marangoni boundary layers in some papers by Napolitano and Russo [5], Golia and Viviani [6, 7], Napolitano et al. [8] and Pop et al. [9].

As mentioned by Christopher and Wang [10], Marangoni flow induced by surface tension variations along a liquid surface causes undesirable effects in crystal growth melts in the same manner as buoyancy-induced natural convection [11]. These undesirable effects also occur in space-based crystal growth experiments since Marangoni flow occurs in microgravity as well as in earth gravity. Boiling tests in microgravity have shown that the effect of Marangoni flow is significant in microgravity and may be important in earth gravity as well [11, 12].

The numerous investigations of Marangoni flow in various geometries have been reviewed in the literature [13, 14]. Some of the papers most relevant to this work include the order-of-magnitude analysis of Marangoni flow given by Okano et al. [15] that gave the general trends for the variation of the Reynolds number with the Grashof number, Marangoni number, and Prandtl number. Hirata and his co-workers experimentlly and numerically investigated Marangoni flow for various substances in geometries with flat surfaces relevant to this work [13, 15, 16]. Arafune and Hirata [17] presented a similarity analysis for just the velocity profile for Marangoni flow that is very similar to this derivation but the results are effectively limited to surface tension variations that are linearly related to the surface position. Slavtchev and Miladinova [18] presented similarity solutions for surface tension that varied as a quadratic function of the temperature as would occur near a minimum. Schwabe and Metzger [19] experimentally investigated Marangoni flow on a flat surface combined with natural convection in a unique geometry where the Marangoni effect and the buoyancy effect could be varied independently.

This paper presents a similarity solution for Marangoni flow over a flat surface due to imposed temperature and concentration gradients. The analysis assumes that the surface tension varies linearly with temperature and concentration but the wall temperature and concentration variations are quadratic functions of the location. Napolitano et al. [20] considered double-diffusive boundary layer along a vertical free surface. As mentioned by Christopher and Wang [10], for an interface with evaporation or condensation at the surface, the temperature distribution along the interface is primarily a function of the vapor temperature and the heat transfer coefficient rather than the Marangoni flow. For example, Christopher and Wang [21] showed that the calculated temperature distribution in vapor bubble attached to a surface and in the liquid surrounding the bubble was primarily due to the heat transfer through the vapor rather than in the liquid region and the temperature variation along the surface was not linear but could be described by a power-law function.

2 Mathematical formulation

Consider steady laminar boundary layer flow of an electrically-conducting fluid over a flate surface in the presense of surface tension due to temperature and concentration gradients at the wall. A uniform magnetic field is assumed to exist in the direction normal to the surface. The surface is assumed to be permeable so as to allow for possible suction or injection at the wall. Heat generation or absorption as well as a first-order chemical reaction effects are assumed to exist. The surface temperature and concentration are assumed to be quadratic functions of the distance alog the surface. Unlike the Boussineq effect in buoyancy-induced flow, the Marangoni effect acts as a boundary condition on the governing equations for the flow field. Taking the above assumptions into consideration, the governing equations for this investigation are based on the balance laws of mass, linear momentum, energy and concentration species. These can be written in dimensional form as:

$$\frac{\partial u}{\partial x}+\frac{\partial v}{\partial y}=0 \tag{1}$$

$$u\frac{\partial u}{\partial x}+v\frac{\partial u}{\partial y}=\nu\frac{\partial^2 u}{\partial y^2}-\frac{\Delta B_0^2}{\rho}u \tag{2}$$

$$u\frac{\partial T}{\partial x}+v\frac{\partial T}{\partial y}=\alpha\frac{\partial^2 T}{\partial y^2}+\frac{Q_0}{\rho c_p}(T-T_\infty) \tag{3}$$

$$u\frac{\partial c}{\partial x}+v\frac{\partial c}{\partial y}=D\frac{\partial^2 c}{\partial y^2}-R(c-c_\infty) \tag{4}$$

The dependence of surface tension on temperature and concentration can be expressed as

$$\sigma=\sigma_0[1-\gamma_T(T-T_\infty)-\gamma_c(c-c_\infty)] \tag{5}$$

where

$$\gamma_{\mathrm{T}}=\left.\frac{\partial\sigma}{\partial T}\right|_{\mathrm{c}},\quad \gamma_c=\left.\frac{\partial\sigma}{\partial c}\right|_{\mathrm{T}} \tag{6}$$

The dimensional boundary conditions for this problem can be written as

$$\mu\left.\frac{\partial u}{\partial y}\right|_{y=0}=-\left.\frac{\mathrm{d}\sigma}{\mathrm{d}T}\right|_{\mathrm{c}}\left.\frac{\partial T}{\partial x}\right|_{y=0}-\left.\frac{\mathrm{d}\sigma}{\mathrm{d}c}\right|_{\mathrm{T}}\left.\frac{\partial c}{\partial x}\right|_{y=0} \tag{7a}$$

$$v(x,0)=-v_0,\quad T(x,0)=T_\infty+Ax^2,\quad c(x,0)=c_\infty+A^*x^2 \tag{7b}$$

$$u(x,\infty)=0,\quad T(x,\infty)=T_\infty,\quad c(x,\infty)=c_\infty \tag{7c}$$

Using the standard definition of the stream function such that $u=\partial\psi/\partial y$ and $v=-\partial\psi/\partial x$ and introducing the following similarity variables:

$$\eta=C_1y,\ f(\eta)=C_2x^{-1}\psi(x,y),\quad \theta(\eta)=\frac{[T(x,y)-T_\infty]x^{-2}}{A},\ C(\eta)=\frac{[c(x,y)-c_\infty]x^{-2}}{A^*} \tag{8}$$

where

$$C_1=\sqrt{[3]}\frac{\rho A(\mathrm{d}\sigma/\mathrm{d}T)|_{\mathrm{c}}}{\mu^2},\ C_2=\sqrt{[3]}\frac{\rho^2}{\mu A(\mathrm{d}\sigma/\mathrm{d}T)|_{\mathrm{c}}} \tag{9}$$

into Eqs. 1, 2, 3 and 4 yields

$$f'''+ff''-f'^2-M^2f'=0 \tag{10}$$

$$\theta''+Pr(f\theta'-2f'\theta)+Pr\phi\theta=0 \tag{11}$$

$$C''+Sc(fC'-2f'C)-ScKC=0 \tag{12}$$

The dimensionless form of the boundary conditions become

$$f''(0)=-2(1+r),\quad f(0)=f_0,\quad \theta(0)=1,\quad C(0)=1$$
$$f'(\infty)=0,\quad \theta(\infty)=0,\quad C(\infty)=0 \tag{13a - g}$$

where $r=.\ (d\sigma/dc)\ |_T\ \Delta c/[.\ (d\sigma/dT)\ |_c\ \Delta T]$ is the thermo-solutal surface tension ratio. It should be mentioned that when $r=0$, Eq. 13a does not reduce to that of Christopher and Wang [10] as they have missed a term in their equation. Their equation should read $f''(0)=-\ (1+k)$ and not $f''(0)=-\ 1$. Therefore, the results they reported for k ≠ 0 are not correct.

Based on Eq. 8, the surface velocity is given by

$$u(x,0)=\sqrt{[3]}\frac{[A(\mathrm{d}\sigma/\mathrm{d}T)|_{\mathrm{c}}]^2}{\rho\mu}xf'(0) \tag{14}$$

It is seen that the surface velocity is proportional to f'(0). The temperature and concentration gradient coefficients (A and A^*) can be defined along a surface of length L as follows:

$$A=\frac{\Delta T}{L^2},\quad A^*=\frac{\Delta c}{L^2} \tag{15}$$

Two Marangoni numbers can be defined based on a surface length L. These are the thermal Marangoni number $Ma_{\mathrm{L,T}}$ and the solutal Marangoni number $\mathrm{Ma_{L,c}}$. They are defined as

$$Ma_{\mathrm{L,T}}=\frac{(\mathrm{d}\sigma/\mathrm{d}T)|_{\mathrm{c}}L\Delta T}{\mu\alpha},\quad Ma_{\mathrm{L,c}}=\frac{(\mathrm{d}\sigma/\mathrm{d}c)|_{\mathrm{T}}L\Delta c}{\mu\alpha} \tag{16}$$

such that

$$r=\frac{Ma_{\mathrm{L,c}}}{Ma_{\mathrm{L,T}}} \tag{17}$$

As done by Christopher and Wang [10], the Reynolds number based on a surface length L is given in terms of the thermal Marangoni number as

$$Re_{\mathrm{L}}=\frac{u(x,0)L}{\nu}=Ma_{\mathrm{L,T}}^{2/3}Pr^{-2/3}f'(0) \tag{18}$$

The total mass flow in the boundary layer per unit width is related to $f(\infty)$ as follows:

$$\mathring{m} = \int_0^\infty \rho u \, \mathrm{d}y = \sqrt{[3]}A(\mathrm{d}\sigma/\mathrm{d}T)|_c \rho\mu x f(\infty) \tag{19}$$

This can be written in dimensionless form for an arbirary surface length x as

$$\overline{Re_x} = \frac{\rho\overline{u}\delta}{\mu} = Ma_{x,T}^{1/3} Pr^{-1/3} f(\infty) \tag{20}$$

The similarity transformations used here are similar to those used previously by Christopher and Wang [10] for k = 1. However, the one used herein for the momentum equation differs in several ways from that used by Arafune and Hirata [17]. Besides slightly different definitions of the similarity variables, the most important difference is that the present similarity transformation is based on the quadratic form of the temperature variation on the surface. The results of Arafune and Hirata [17] are only useful for a linear variation of the surface tension with location. The current derivation is also extended to include the energy and concentartion equations.

The present analysis follows closely that of Christopher and Wang [10]. Thus, the same assumptions reported by them are valid. Among these assumptions is the fact that the similarity analysis is based on the boundary layer equations which assume that the tranverse derivatives of the velocity, temperature and concentration are much larger than their axial derivatives and that the axial velocity is much larger than the trasverse velocity. Analysis of the similarity transformation shows that these assumptions are true if

$$C_1 L = \sqrt{[3]}\frac{\rho A L^3 (\mathrm{d}\sigma/\mathrm{d}T)\big|_c}{\mu^2} = Ma_{L,T}^{1/3} Pr^{-1/3} >> 1 \tag{21}$$

3 Heat and mass transfer effects

It is possible to obtain approximate analytical solutions for both the energy and concentration equations depending on the order of magnitude of both the Prandtl and Schmidt numbers. For example, for small Prandtl numbers, the thermal boundary-layer thickness is much greater than that of the momentum boundary layer. In this case, $f'(\eta)$ is essentially zero over most of the domain and the $f(\eta)$ can be replaced by $f(\infty)$. The same is true for the concentration equation or small values of Schmidt numbers. Taking these facts into consideration, the energy and concentration equations can be approximated by:

$$\theta'' + Prf(\infty)\theta' + Pr\phi\theta = 0 \tag{22}$$
$$C'' + Scf(\infty)C' - ScKC = 0 \tag{23}$$

Without going into detail, it can be shown that the solutions of the above two equations subject to the appropriate boundary conditions in Eq. 13 are

$$\theta(\eta) = \exp\left\{-\left[(Prf(\infty) + \sqrt{Pr^2 f(\infty)^2 - 4Pr\phi})/2\right]\eta\right\} \tag{24}$$

$$C(\eta) = \exp\left\{-\left[(Scf(\infty) + \sqrt{Sc^2 f(\infty)^2 + 4ScK})/2\right]\eta\right\} \tag{25}$$

The wall temperature and concentration gradients for small Pr and Sc values are given by

$$\theta'(0) = -(Pr\, f(\infty) + \sqrt{Pr^2 f(\infty)^2 - 4Pr\phi})/2 \tag{26}$$
$$C'(0) = -(Scf(\infty) + \sqrt{Sc^2 f(\infty)^2 + 4ScK})/2 \tag{27}$$

Eqs. 24 and 26 reduce to the same equations reported by Christopher and Wang [10] for $k = 1$ when ϕ is equated to zero.

For large Prandtl and Schmidt numbers, the thermal and concentration boundary layer thicknesses are much thinner than that of the momentum boundary layer. In this case, $f(\eta)$ is essentially zero over most of the domain and the $f'(\eta)$ can be replaced by $f'(0)$ for small values of η. Taking these facts into consideration, the energy and concentration equations can then be approximated by:

$$\theta'' - 2Prf'(0)\theta - Pr\phi\theta = 0 \tag{28}$$
$$C'' - 2Scf'(0)C - ScKC = 0 \tag{29}$$

It can be shown that the solutions of the above two equations subject to the appropriate boundary conditions in Eq. 13 can be written as

$$\theta(\eta) = \exp(-\sqrt{2Prf'(0) - Pr\phi}\,\eta) \tag{30}$$
$$C(\eta) = \exp(-\sqrt{2Scf'(0) + ScK}\,\eta) \tag{31}$$

The corresponding temperature and concentration gradients at the surface are given by

$$\theta'(0) = -\sqrt{2Prf'(0) - Pr\phi} \tag{32}$$
$$C'(0) = -\sqrt{2Scf'(0) + ScK} \tag{33}$$

Again, Eqs. 30 and 32 reduce to the same equations reported by Christopher and Wang [10] for $k = 1$ when ϕ is equated to zero.

The local Nusselt and Sherwood numbers are given by

$$Nu_x = \frac{q''(x)x}{\lambda[T(x,0) - T_\infty]} = -C_1 x\theta'(0) \tag{34}$$

$$Sh_x = \frac{c''(x)x}{D[c(x,0) - c_\infty]} = -C_1 xC'(0) \tag{35}$$

For small Prandtl and Schmidt numbers, it can be shown based on the approximate analytical solutions (26) and (27) that

$$Nu_x = -Ma_{L,T}^{1/3} Pr^{-1/3}(x/L)\theta'(0)$$
$$= Ma_{L,T}^{1/3} Pr^{-1/3}(x/L)(Pr\, f(\infty) + \sqrt{Pr^2 f(\infty)^2 - 4Pr\phi})/2 \quad (36)$$
$$Sh_x = -Ma_{L,T}^{1/3} Pr^{-1/3}(x/L)C'(0)$$
$$= Ma_{L,T}^{1/3} Pr^{-1/3}(x/L)(Scf(\infty) + \sqrt{Sc^2 f(\infty)^2 + 4ScK})/2 \quad (37)$$

For large Prandtl and Schmidt numbers, it can be shown based on the approximate analytical solutions (32) and (33) that

$$Nu_x = -Ma_{L,T}^{1/3} Pr^{-1/3}(x/L)\theta'(0)$$
$$= Ma_{L,T}^{1/3} Pr^{-1/3}(x/L)\sqrt{2Pr\, f'(0) - Pr\, \phi} \quad (38)$$
$$Sh_x = -Ma_{L,T}^{1/3} Pr^{-1/3}(x/L)C'(0)$$
$$= Ma_{L,T}^{1/3} Pr^{-1/3}(x/L)\sqrt{2Scf'(0) + ScK} \quad (39)$$

It should be noted that Eqs. 36 and 38 reduce to the same equations reported by Christopher and Wang [10] for $k = 1$ when ϕ is equated to zero.

4 Numerical method

Equations 10, 11, 12 subject to the boundary conditions (13) have been solved numerically using the implicit finite-difference method discussed by Blottner [22] for the Prandtl number $Pr = 0.78$ corresponding to metal ammonia suspension and the Schmidt number $Sc = 0.6$ corresponding to water vapor. These equations are discretized using three-point central-difference quotients and, as a consequence, a set of algebraic equations results. The corresponding algebraic equations are then solved by the well-known tri-diagonal Thomas algorithm (see Blottner [22]). The computational domain was divided into 195 nodal points and variable step sizes were utilized. The initial step size $\Delta\eta_1$ and the growth factor K^* employed in the present work were 0.001 and 1.04, respectively such that $\Delta\eta_{j+1} = K^* \Delta\eta_j$ where the subscript "j" denotes nodal point location. The edge of the boundary layer was represented by $\eta_\infty = 50$. These step sizes were found to give accurate grid-independent results as verified by comparisons (not shown here for brevity) with the results of Christopher and Wang [10] for $k = 0$. The iteration criterion employed was based on the relative difference between the current and the previous iterations. When this difference reached 10^{-5} for all of the dependent variables, the solution was assumed converged and the iteration procedure was terminated.

5 Results and discussion

In this section, a representative set of graphical and tabulated results is presented in Figs. 1, 2, 3, 4, 5, 6, 7, 8, 9, 10, 11, 12 and 13 and Tables 1, 2, 3, 4, 5 and 6 to illustrate the influence of the various physical parameters on the solutions.

Figs. 1, 2 and 3 present typical velocity, temperature and concentration profiles for various values of the Hartmann number M, respectively. Application of a transverse magnetic field results in a drag-like force called the Lorentz force. This force tends to slow down the movement of the fluid along surface and to increase its temperature and the concentration species. This is evident in the decreases in the velocities and increases in the temperature and concentration as M increases. In addition, as the strength of the magnetic field increases, the hydrodynamic boundary layer decreases while the thermal and solutal (concentration) boundary layer. It is also observed from Fig. 1 that the wall velocity is non-zero due to the Marangoni or surface tension effect and it decreases as M increases. These behaviors are depicted in Figs. 1, 2 and 3.

Figs. 4, 5 and 6 illustrate the influence of the suction or injection parameter f_0 on the velocity, temperature and concentration profiles, respectively. Physically speaking, imposition of fluid suction ($f_0 > 0$) at the wall has the tendency to decrease the fluid velocity and the hydrodynamic boundary layer. As a result, the fluid temperature and concentration species and their boundary layers decrease as well. However, fluid wall blowing or injection ($f_0 < 0$) produces the opposite effect, namely increases in the fluid velocity, temperature and concentration species.

These trends are obvious from Figs. 4, 5 and 6.

Figure 7 depicts the effect of the heat generation or absorption coefficient ϕ on the temperature profiles. In general, while heat absorption has a tendency to cool down the fluid temperature, heat generation increases it. However, for the parametric values employed to produce this figure, significant heat generation causes a

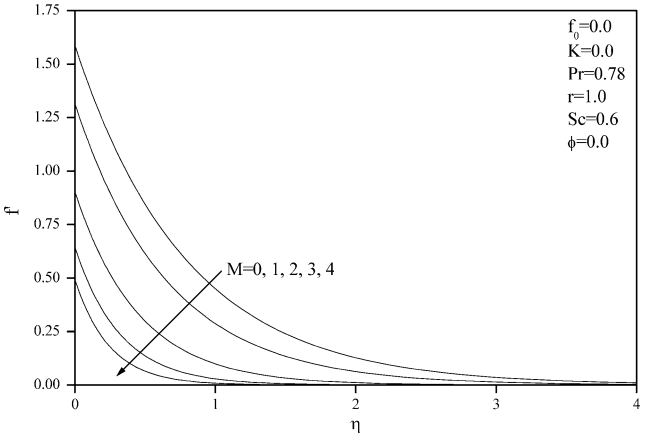

Fig. 1 Effects of M on velocity profiles

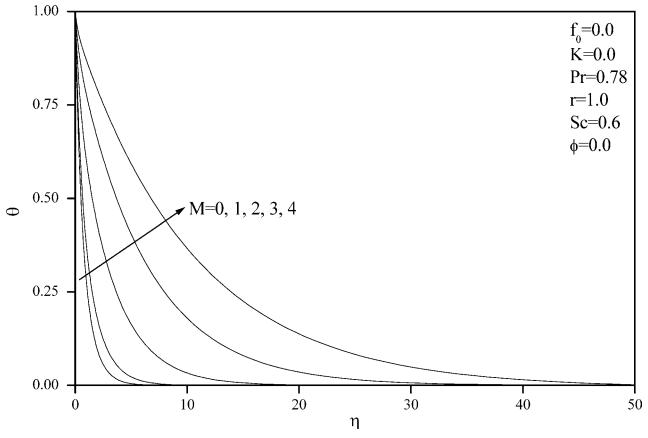

Fig. 2 Effects of M on temperature profiles

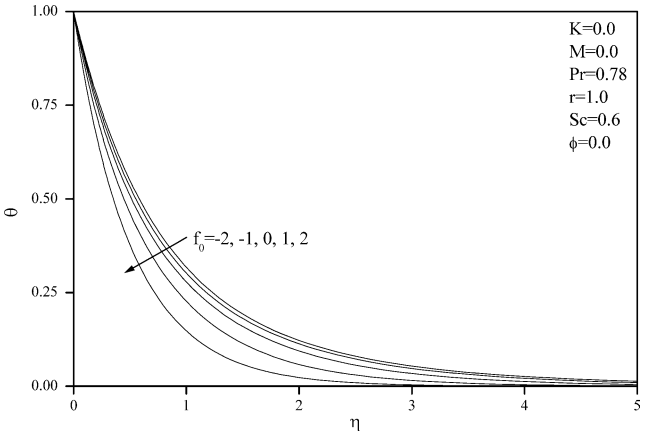

Fig. 5 Effects of f_0 on temperature profiles

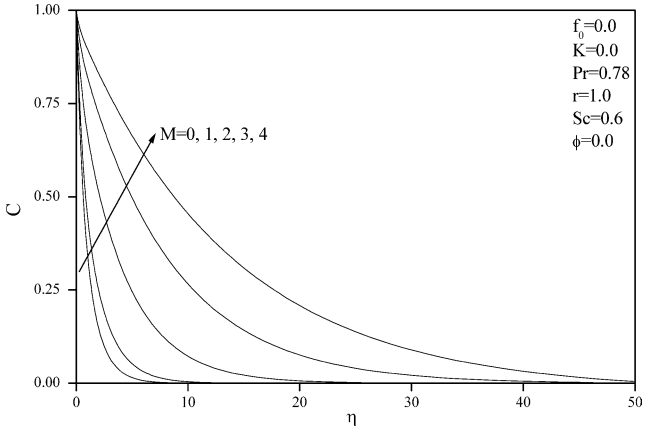

Fig. 3 Effects of M on concentration profiles

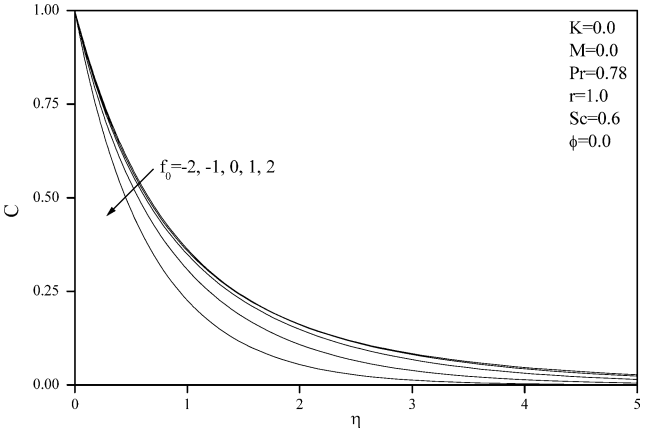

Fig. 6 Effects of f_0 on concentration profiles

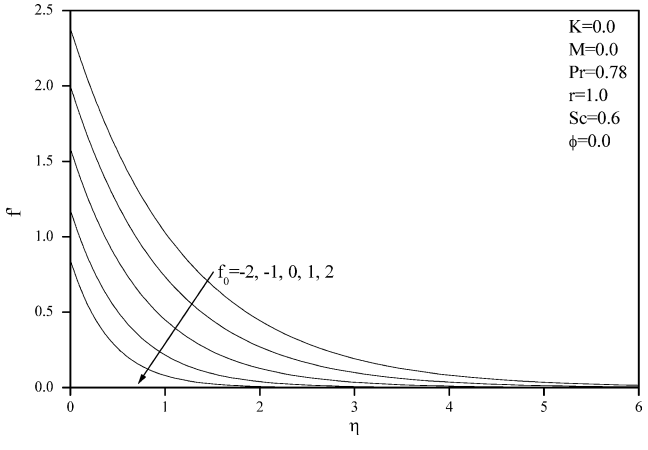

Fig. 4 Effects of f_0 on velocity profiles

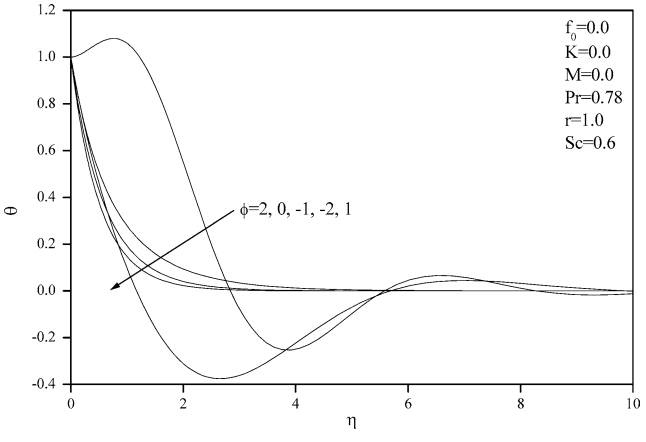

Fig. 7 Effects of ϕ on temperature profiles

temperature deficit where the fluid temperature goes below that of the free stream and oscillates thereafter until it reaches the free stream value.

In Figs. 8, 9 and 10, the influence of the thermo-solutal surface tension ratio r on the profiles of velocity, temperature and concentration is presented, respectively. As r increases, the Marangoni convection effect increases causing more induced flow. This induced flow starts at the surface and propagates in the boundary layer. Thus, the maximum velocity occurs at the wall. However, this increase in velocity due to the increase in Marangoni convection effect is followed with simultaneous decreases in both the fluid temperature and con-

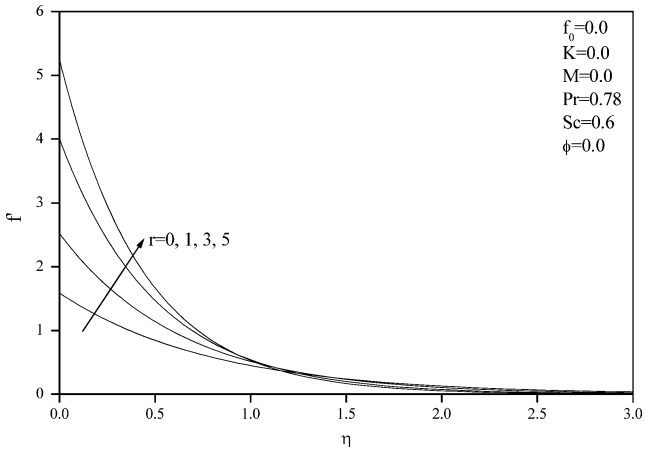

Fig. 8 Effects of r on velocity profiles

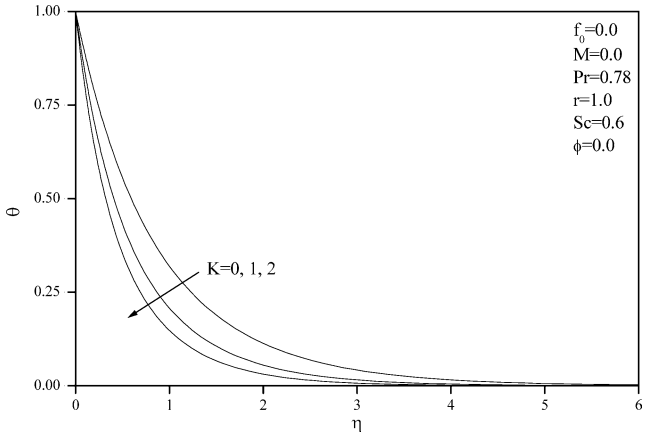

Fig. 11 Effects of K on temperature profiles

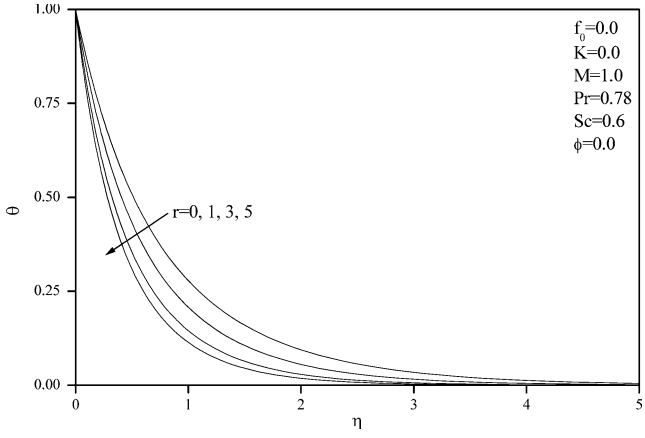

Fig. 9 Effects of r on temperature profiles

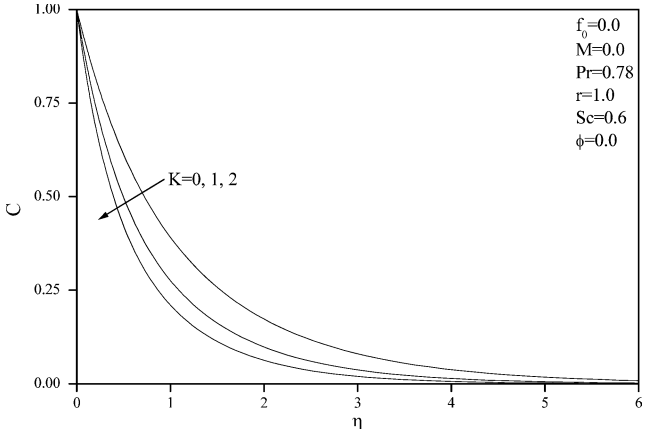

Fig. 12 Effects of K on concentration profiles

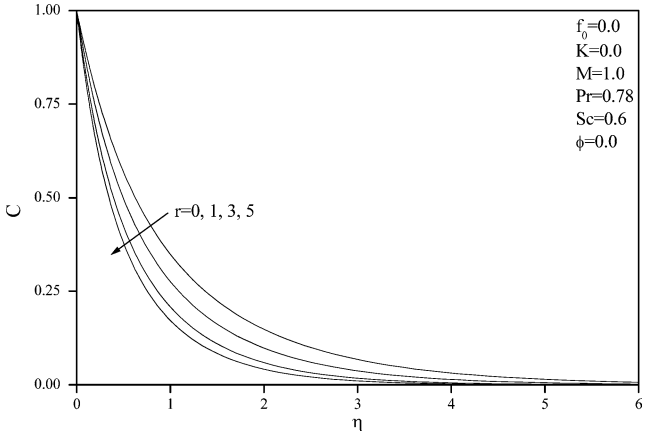

Fig. 10 Effects of r on concentration profiles

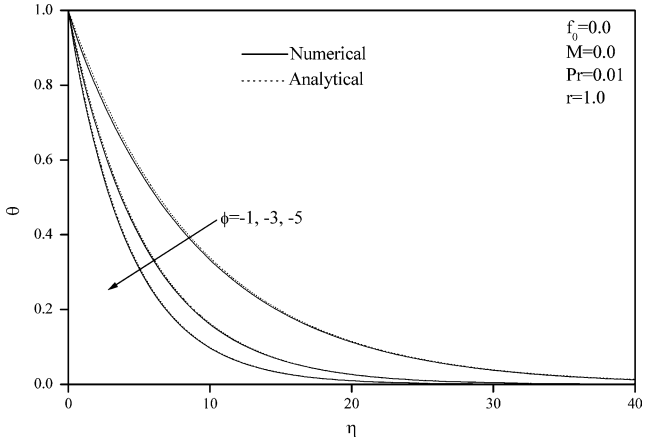

Fig. 13 Comparison of numerical and analytical temperature profiles

centration species. These trends are illustrated clearly in Figs. 8, 9 and 10.

Figs. 11 and 12 display the effect of the chemical reaction coefficient K on the temperature and concentration profiles, respectively. Inspection of the chemical reaction term (last term) of Eq. 12 and the last term of Eq. 11 shows that increases in the value of K have the same effect on the concentration profile as that of the heat absorption on the temperature profile. Namely, as K increases the concentration level decreases. In

addition, it is predicted that as K increases, the fluid temperature decreases as well. These behaviors are obvious from Figs. 11 and 12.

Figure 13 shows a comparison between the approximate analytical results for the temperature field based on Eq. 24 and the numerical results for small Pr values. It is evident from this figure that excellent agreement exists for all values of ϕ considered. It should be noted that the same conclusion is valid for the concentration field since the concentration equation is similar to the energy equation with a heat sink (absorption).

Tables 1, 2, 3, 4 and 5 illustrate the influence of the Hartmann number M, the suction or injection parameter f_0, the heat generation or absorption coefficient ϕ, the thermo-solutal surface tension ratio r and the chemical reaction coefficient K on the physical parameters $f'(0)$, $f(\infty)$, $-\theta'(0)$ and $-C'(0)$. It can be seen from Table 1 that all of $f'(0)$, $f(\infty)$, $-\theta'(0)$ and $-C'(0)$ decrease as M increases. Table 2 shows that all of $f(\infty)$, $-\theta'(0)$ and $-C'(0)$ increase while $f'(0)$ decreases as f_0 increases. Table 3 shows that the effect of ϕ is limited to $-\theta'(0)$ which decreases as ϕ increases. Table 4 shows that 0all of $f'(0)$, $f(\infty)$, $-\theta'(0)$ and $-C'(0)$ increase as r increases. Finally, Table 5 indicates that as K increases all of $f'(0)$, $-\theta'(0)$ and $-C'(0)$ increase while $f(\infty)$ decreases. It should be mentioned that the increase or decrease of $f'(0)$, $f(\infty)$, $-\theta'(0)$ and $-C'(0)$ should be related to the surface velocity, total mass flow in the boundary layer, Nusselt number and Sherwood numbers, respectively.

Table 6 shows comparisons of approximate analytical Eqs. 32 and 33 and numerical results of $-\theta'(0)$ and $-C'(0)$ for large values of Prandtl number ($Pr = 10$) and large values of Schmidt number ($Sc = 10$) and various values of ϕ and K. It can be seen that the comparisons are good. The errors in comparisons are attributed to the fact that the assumptions on $f(\eta)$ and $f'(\eta)$ used to

Table 1 Effects of M on f'(0), $f(\infty)$, $-\theta'(0)$ and $-C'(0)$

M	f'(0)	f(∞)	-θ'(0)	−C'(0)
0	1.587671	1.259247	1.442203	1.220880
1	1.315181	0.8641415	1.206468	1.005541
2	0.9039450	0.4081968	0.7596045	0.6106418
3	0.6448883	0.2076675	0.4422402	0.3473967
4	0.4933589	0.1214920	0.2728471	0.2127706

Table 2 Effects of f_0 on$f'(0)$, $f(\infty)$, $-\theta'(0)$ and $-C'(0)$

f_0	$f'(0)$	$f(\infty)$	$-\theta'(0)$	$-C'(0)$
−2	2.383451	0.8387348	1.251341	1.129218
−1	2.000379	0.9993013	1.336441	1.173002
0	1.587671	1.259247	1.442203	1.220880
1	1.179708	1.695019	1.634990	1.328699
2	0.8480268	2.359058	2.020945	1.593570

Table 3 Effects of ϕ on $f'(0)$, $f(\infty)$, $-\theta'(0)$ and $-C'(0)$

ϕ	$f'(0)$	f(∞)	$-\theta'(0)$	−C'(0)
−2	1.587671	1.259247	1.973585	1.220880
−1	1.587671	1.259247	1.739584	1.220880
0	1.587671	1.259247	1.442203	1.220880
1	1.587594	1.259018	1.387539	1.220880
2	1.587594	1.258998	−9.5255515E-03	1.220880

Table 4 Effects of r on f'(0), f(∞), $-\theta'(0)$ and −C'(0)

r	f'(0)	f(∞)	$-\theta'(0)$	−C'(0)
0	1.587582	1.259386	1.442247	1.220880
1	2.520988	1.586534	1.817826	1.538960
3	4.001780	1.998838	2.290178	1.938865
5	5.244303	2.288324	2.621562	2.219093

Table 5 Effects of K on f'(0), f(∞), $-\theta'(0)$ and $-C'(0)$

K	$f'(0)$	F(∞)	$-\theta'(0)$	$-C'(0)$
0	2.057155	1.865242	1.211093	1.024810
1	2.520988	1.586534	1.817826	1.538960
2	2.857944	1.423707	2.335740	1.977876

Table 6 Comparisons of analytical and numerical solutions for $-\theta'(0)$ and -C'(0) for large Pr and Sc values, $f_0 = 0$, M = 0, Pr = 10, r = 0 and Sc = 10

ϕ	$-\theta'(0)$ Analytical	$-\theta'(0)$ Numerical	K	$-C'(0)$ Analytical	$-C'(0)$ Numerical
0	5.634999	6.045044	0	5.634999	6.045044
−1	6.461693	6.843566	1	6.461693	6.843566
−2	7.193987	7.553650	2	7.193987	7.553650
−3	7.858298	8.199263	3	7.858298	8.199263
−5	9.041734	9.353470	5	9.041734	9.353470

obtain the approximate analytical solutions (32) and (33) are not totally correct near the wall which in turn affects the wall temperature and concentration gradients.

6 Conclusions

Thermo-solutal Marangoni convection flow of an electrically-conducting fluid along a vertical permeable surface in the presence of a magnetic field, heat generation or absorption and a first-order chemical reaction effects was analyzed numerically. The general governing partial differential equations were converted into a set of self-similar equations using unique similarity transformations. Numerical solution of the similarity equations was obtained using an implicit, iterative, tri-diagonal finite-difference method. Comparisons with previously published work was performed and the results were found to be in excellent agreement. The effects of Hartmann number, heat generation or absorption coefficient, the suction or injection parameter, the thermo-solutal surface tension ratio and the chemical reaction coefficient on the velocity, temperature and concentration profiles as well as quantitites related to the wall velocity, boundary-layer mass flow rate and the Nusselt and Sherwood numbers were presented in graphical and tabular form and discussed. It was found that a first-order chemical reaction increased all of the wall velocity, Nusselt and Sherwood numbers while it decreased the mass flow rate in the boundary layer. Also, as the thermo-solutal surface tension ratio was increased, all of the wall velocity, boundary-layer mass flow rate and the Nusselt and Sherwood numbers were increased. However, the exact opposite behavior was predicted as the magnetic field strength was increased. It should be noted that results obtained in this work can be used for the analysis of Marangoni flow and heat and mass transfer for flow over curved surfaces provided that the curvature is much greater than the boundary layer thickness.

References

1. Napolitano LG (1978) Microgravity fluid dynamics. In: 2nd Levitch conference, Washington
2. Napolitano LG (1979) Marangoni boundary layers. In: Proceedings of the 3rd European symposium on material science in space. Grenoble, ESA SP-142, June 1979
3. Napolitano LG (1982) Surface and buoyancy driven free convection, Acta Astronautica 9:199–215
4. Napolitano LG, Golia C (1981) Coupled Marangoni boundary layers. Acta Astronautica 8:417–434
5. Napolitano LG, Russo G (1984) Similar axially symmetric Marangoni boundary layers, Acta Astronautica 11:189–198
6. Golia C, Viviani A (1985) Marangoni buoyant boundary layers. L'Aerotechnica Missili e Spazio 64:29–35
7. Golia C, Viviani A (1986) Non isobaric boundary layers related to Marangoni flows. Meccanica 21:200–204
8. Napolitano LG, Carlomagno GM, Vigo P (1977) New classes of similar solutions for laminar free convection problems, Int J Heat Mass Transfer 20:215–226
9. Pop I, Postelnicu A, Grosan T (2001) Thermosolutal Marangoni forced convection boundary layers. Meccanica 36:555–571
10. Christopher DM, Wang B (2001) Prandtl number effects for Marangoni convection over a flat surface. Int J Therm Sci 40:564–570
11. Eyer A, Leist H, Nitsche R (1985) Floating zone growth of silicon under microgravity in sounding rocket. J Crystal Growth 71:173–182
12. Straub J (1994) The role of surface tension for two phase heat and mass transfer in the absence of gravity. Exp Therm Fluid Sci 9:253–273
13. Arafune K, Hirarta A (1998) interactive solutal and thermal Marangoni convection in a rectangular open boat. Numer Heat Tran Part A 34:421–429
14. Croll A, Muller-Sebert W, Nitsche R (1989) The critical Marangoni number for the onest of time-dependent convection in silicon. Mater Res Bull 24:995–1004
15. Okano Y, Itoh M, Hirata A (1989) Natural and Marangoni convections in a two-dimensional rectangular open boat. J Chem Eng Japan 22:275–281
16. Arafune K, Sugiura M, Hirata A (1999) Investigation of thermal Marangoni convection in low and high Prandtl number fluids. J Chem Eng Japan 32:104–109
17. Arafune K, Hirata A (1999) Thermal and solutal Marangoni convection in In-Ga-Sb system. J Crystal Growth 197:811–817
18. Slavtchev S, Miladinova S (1998) Thermocapillary flow in a liquid layer at minimum in surface tension. Acta Mech 127:209–224

19. Schwabe D, Metzger J (1989) Coupling and separation of buoyant and thermocapillary convection. J Crystal Growth 97:23–33
20. Napolitano LG, Viviani A, Savino R (1992) Double-diffusive boundary layers along vertical free surfaces. Int J Heat Mass Transfer 35:1003–1025
21. Christopher D, Wang B (1998) Marangoni convection around a bubble in microgravity, heat transfer. In: Lee JS(ed) proceedings of the 11th international heat transfer conference, Vol 3. Taylor & Francis, Levittown, pp 486–494
22. Blottner FG (1970) Finite-difference method of solution of the boundary layer equations. AIAA J 8:193–205